Scanning Tunneling Microscopy Investigations of the Local Electronic and Structural Effects of Iron Substitution in Tantalum Disulfide

Huifen Chen, Xian Liang Wu, and Charles M. Lieber*

Contribution from the Department of Chemistry, Columbia University, New York, New York 10027. *Received October 30, 1989*

Abstract: The microscopic structural and electronic properties of the charge density wave (CDW) phases in a series of iron-substituted tantalum disulfide materials, $Fe_xTa_{1-x}S_2$, have been characterized with the use of scanning tunneling microscopy (STM). On average, the incommensurate CDW phase exhibits a regular hexagonal superlattice for $x(Fe) \leq 0.02$. At the atomic level, however, analysis of real-space STM images shows that there are well-defined defects in this CDW structure. The frequency and size of the defects depend directly on the concentration of iron. Furthermore, atomic resolution images demonstrate that these defects involve a spatially localized CDW amplitude distortion or coupled amplitude–position distortion. For $x(Fe) \geq 0.04$ the CDW superlattice exhibits large distortions in the wavelength and amplitude. The distortions in the CDW structure have been characterized as a function of iron concentration by real-space wavelength measurements and two-dimensional Fourier transform power spectra of the images. These results resolve the source of differences between STM and previous diffraction studies of metal-substituted tantalum disulfide and also indicate that above a critical concentration of iron the properties of the CDW phase in these materials change significantly. The origin of this critical concentration is discussed.

Understanding the factors that determine the structure, electronic properties, and phase transitions in materials is an important objective of researchers in solid-state chemistry and physics.[1] One chemical approach used to probe these key properties involves the preparation of a series of materials in which one or more sites are systematically varied.[2-7] Previously, the structures of such chemically modified materials have been studied with diffraction techniques (i.e., X-ray, electron, and neutron), while the electronic properties have been investigated with photoelectron spectroscopy and transport measurements. These conventional techniques typically probe a macroscopic portion of a sample and, hence, provide results that reflect the average structural and electronic properties of a material. It is especially important when assessing the effects of chemical modification in materials to also characterize these properties at the atomic level. A new technique that has shown promise in providing this important local information is scanning tunneling microscopy (STM).[8-13] In this paper we describe STM investigations of the local electronic and structural effects of iron substitution on the charge density wave (CDW) phases in octahedrally coordinated tantalum disulfide (1T-TaS_2).

Tantalum disulfide is a quasi-two-dimensional material that consists structurally of strongly bonded sulfur–tantalum–sulfur layers that are held together predominantly by weak van der Waals interactions between adjacent sulfur planes (Figure 1A).[14] The sulfur atoms are arranged in hexagonal close-packed planes with the tantalum centers in octahedral holes. Electronically, this d^1 system is metallic at high temperatures; however, on cooling below 543 K the ground state of 1T-TaS_2 is a CDW state.[14] A CDW is a simultaneous periodic distortion of the conduction electron density and atomic lattice. For tantalum disulfide the lattice distortions are ≤ 0.2 Å while the period of the charge modulation is ≈ 12 Å. Four distinct temperature-dependent CDW phases have been proposed for 1T-TaS_2 on the basis of diffraction and transport measurements.[14,15] On cooling, the high-temperature incommensurate phase undergoes a first-order transition at 353 K to a nearly commensurate state, which subsequently undergoes a transition to a commensurate phase at 183 K; warming from the commensurate state produces the fourth triclinic nearly commensurate phase at 223 K, which undergoes a transition back to the nearly commensurate state at 283 K. These CDW phases can be distinguished from each other by the amplitude and phase of the charge modulation relative to the lattice, as discussed elsewhere.[14-16] These phases can be perturbed by metal substitution (Figure 1B). Previously, the effects of metal substitution on the CDW phases in several $M_xTa_{1-x}S_2$ materials have been probed with diffraction and transport methods.[7,14,17] More recently, we have reported[10-12,18] the first STM studies of several chemically modified materials. Notably, our preliminary studies have shown that the atomic scale electronic and structural properties of the metal-substituted materials, which are determined directly by STM, can differ significantly from those inferred by

(1) (a) *Physics Through the 1990s: Condensed-Matter Physics*; National Academy Press: Washington, DC, 1986. (b) *Opportunities in Chemistry*; National Academy Press: Washington, DC, 1985.
(2) Liou, K.; Jacobsen, C. S.; Hoffman, B. M. *J. Am. Chem. Soc.* **1989**, *111*, 6616.
(3) Almeida, M.; Gaudiello, J. G.; Kellogg, G. E.; Tetrick, S. M.; Marcy, H. O.; McCarthy, W. J.; Butler, J. C.; Kannewurf, C. R.; Marks, T. J. *J. Am. Chem. Soc.* **1989**, *111*, 5271.
(4) Miller, J. S.; Epstein, A. J. *Angew. Chem., Int. Ed. Engl.* **1987**, *26*, 287.
(5) (a) Rao, C. N. R.; Raveau, B. *Acc. Chem. Res.* **1989**, *22*, 106. (b) Sleight, A. W. *Science (Washington)* **1988**, *242*, 1519. (c) Williams, J. M.; Beno, M. A.; Carlson, K. D.; Geiser, U.; Kao, H. C. I.; Kini, A. M.; Porter, L. C.; Shultz, A. J.; Thorn, R. J.; Wang, H. H. *Acc. Chem. Res.* **1988**, *21*, 1. (d) Holland, G. F.; Stacy, A. M. *Acc. Chem. Res.* **1988**, *21*, 8.
(6) (a) Dresselhaus, M. S.; Dresselhaus, G. *Adv. Phys.* **1981**, *30*, 139. (b) Ebert, L. B. *Annu. Rev. Mater. Sci.* **1976**, *6*, 181.
(7) DiSalvo, F. J.; Wilson, J. A.; Bagley, B. G.; Waszczak, J. V. *Phys. Rev. B Solid State* **1975**, *12*, 2220.
(8) (a) Kuk, Y.; Silverman, P. J. *Rev. Sci. Instrum.* **1989**, *60*, 165. (b) Binnig, G.; Rohrer, H. *Angew. Chem., Int. Ed. Engl.* **1987**, *26*, 606. (c) Hansma, P. K.; Tersoff, J. *J. Appl. Phys.* **1987**, *61*, R1.
(9) (a) Coleman, R. V.; McNairy, W. W.; Slough, C. G.; Hansma, P. K.; Drake, B. *Synth. Met.* **1987**, *19*, 881. (b) Slough, C. G.; McNairy, W. W.; Coleman, R. V.; Drake, B.; Hansma, P. K. *Phys. Rev. B Condens. Matter* **1986**, *34*, 994. (c) Coleman, R. V.; Drake, B.; Hansma, P. K.; Slough, G. *Phys. Rev. Lett.* **1985**, *55*, 394.
(10) Wu, X. L.; Lieber, C. M. *J. Am. Chem. Soc.* **1988**, *110*, 5200.
(11) (a) Wu, X. L.; Zhou, P.; Lieber, C. M. *Nature (London)* **1988**, *335*, 55. (b) Wu, X. L.; Zhou, P.; Lieber, C. M. *Phys. Rev. Lett.* **1988**, *61*, 2604.
(12) Wu, X. L.; Lieber, C. M. *J. Am. Chem. Soc.* **1989**, *111*, 2731.
(13) (a) Kelty, S. P.; Lieber, C. M. *J. Phys. Chem.* **1989**, *93*, 5983. (b) Kelty, S. P.; Lieber, C. M. *Phys. Rev. B: Condens. Matter* **1989**, *40*, 5856.
(14) (a) DiSalvo, F. J. In *Electron-Phonon Interactions and Phase Transitions*; Riste, T., Ed.; Plenum: New York, 1977; p 107. (b) Wilson, J. A.; DiSalvo, F. J.; Mahajan, S. *Adv. Phys.* **1975**, *24*, 117.
(15) Bayliss, S. C.; Ghorayeb, A. M.; Guy, D. R. P. *J. Phys. C* **1984**, *17*, L533.
(16) (a) Wu, X. L.; Lieber, C. M. *Science (Washington)* **1989**, *243*, 1703. (b) Wu, X. L.; Lieber, C. M. *Phys. Rev. Lett.*, in press.
(17) (a) DiSalvo, F. J.; Wilson, J. A.; Waszczak, J. V. *Phys. Rev. Lett.* **1976**, *36*, 885. (b) Eibschutz, M.; DiSalvo, F. J. *Ibid.* **1976**, *36*, 104. (c) Fleming, R. M.; Coleman, R. V. *Ibid.* **1975**, *34*, 1502.
(18) Wu, X. L.; Lieber, C. M. *Phys. Rev. B: Solid State* **1990**, *41*, 1239.

0002-7863/90/1512-3326$02.50/0

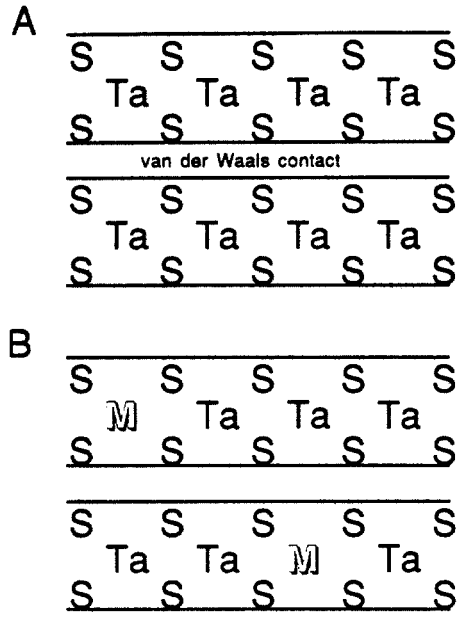

Figure 1. Schematic side view of the structure of (A) TaS_2 and (B) metal-substituted TaS_2, $M_xTa_{1-x}S_2$.

indirect methods (e.g., diffraction). To probe further these interesting results and also to investigate how the chemical nature of the metal center introduced into the lattice affects these local electronic and structural properties, we have carried out a detailed investigation of iron substitution in the tantalum disulfide system. The results of this study are described herein.

Experimental Section.

Crystal Growth. Single crystals of $Fe_xTa_{1-x}S_2$ were prepared from polycrystalline powders by chemical vapor transport.[7] A stoichiometric mixture (5 g) of Fe (99.99+%), Ta (99.9+%), and S (99.999%) was sealed in a quartz tube (1.6 cm (i.d.) × 22 cm) under vacuum ($<10^{-3}$ Torr) and reacted at 950 °C for 10 days. Following reaction, the tubes were rapidly cooled in cold water to ensure that the 1T polymorph was obtained. The polycrystalline powders were then ground and resealed under vacuum in a quartz tube together with excess sulfur (60 mg) and I_2 (180 mg, 99.999%). Crystals were grown in a 50–100 °C gradient with a growth temperature of 870 °C over a 2–3-week period. The crystals obtained from the growth region had the expected platelike morphology and varied in size from 1 × 1 to 5 × 5 mm^2. The stoichiometry of the single crystals was verified by elemental analysis and found in all cases to agree with that of the polycrystalline powder, suggesting that Fe and Ta transport at similar rates. Anal. Calcd for $Fe_{0.01}Ta_{0.99}S_2$: Fe, 0.23; S, 26.30. Found: Fe, 0.22; S, 26.95. Calcd for $Fe_{0.02}Ta_{0.98}S_2$: Fe, 0.46; S, 26.43. Found: Fe, 0.63; S, 26.13. Calcd for $Fe_{0.04}Ta_{0.96}S_2$: Fe, 0.93; S, 26.71. Found: Fe, 0.88; S, 27.02. Calcd for $Fe_{0.08}Ta_{0.92}S_2$: Fe, 1.90; Ta, 70.82; S, 27.28. Found: Fe, 1.75; Ta, 72.10; S, 25.97. Calcd for $Fe_{0.15}Ta_{0.85}S_2$: Fe, 3.70; Ta, 67.96; S, 28.33. Found: Fe, 4.07; Ta, 67.43; S, 29.64. In addition, the surface composition of a single crystal of the $x(Fe) = 0.15$ material was determined with Auger spectroscopy (Physical Electronics) and found to agree with the bulk analysis. The sensitivity of our instrument was insufficient, however, to determine reproducibly the iron concentration in the $x(Fe) \leq 0.08$ materials.

Resistivity Measurements. Four-probe variable-temperature resistivity measurements were made with standard techniques.[19] Electrical contacts to the samples were made with silver paste (Colloidal Silver LQ, Ted Pella, Inc.), and the samples were thermally contacted to the cold stage of a closed-cycle refrigerator (LTS-22, RMC Cryosystems) for temperature control. Resistance and temperature measurements were made under computer control with software developed in our laboratory. Unless otherwise stated, the resistance vs temperature curves were the same for sample cooling and warming.

Scanning Tunneling Microscopy. The scanning tunneling microscope used in these studies is a commercial instrument (Nanoscope, Digital Instruments, Inc.) that has been modified for variable-temperature operation.[16b,20] Images were recorded in the constant-current mode with platinum–iridium (80–20%) alloy tips that were mechanically formed. Experiments were carried out in air and in an argon-filled inert atmosphere glovebox (HE-93, Vacuum Atmospheres) equipped with a purification system for the removal of water and oxygen. In general, the images obtained in air from cleaved crystal surfaces covered with oil and those obtained in inert atmosphere from cleaved surfaces were similar, although for $x(Fe) \geq 0.15$ the crystals appeared to be more stable in the inert atmosphere. The reported bias voltages refer to the sample versus the tip. The calibration of the piezo-tube scanner and the analysis of digital-image data have been described previously.[11,16] The raw-image data were treated with a low-pass filter or a two-dimensional Fourier filter (cutoff ≈2.5 Å). The images obtained from either method were similar.

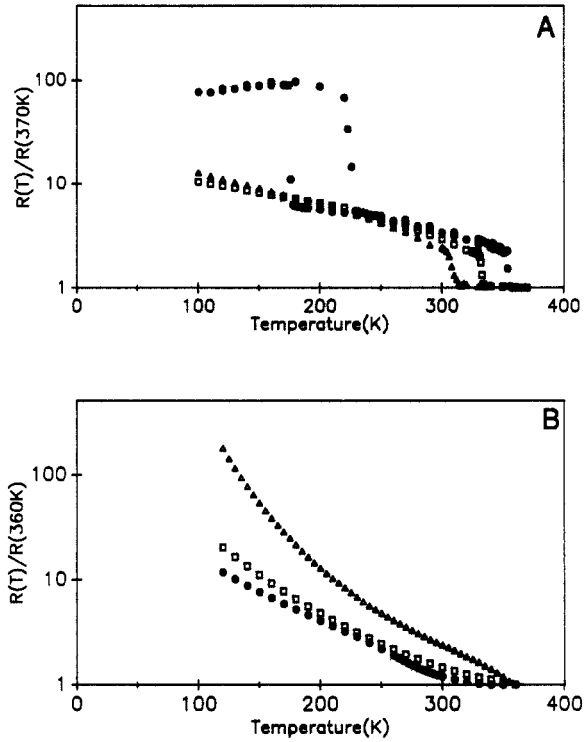

Figure 2. Plots of normalized resistance versus temperature for the $Fe_xTa_{1-x}S_2$ materials: (A) sample resistivity for the $x(Fe) = 0$ (●), $x(Fe) = 0.01$ (□), and $x(Fe) = 0.02$ (△) materials normalized to the value measured at 370 K; (B) sample resistivity for the $x(Fe) = 0.04$ (●), $x(Fe) = 0.08$ (□), and $x(Fe) = 0.15$ (△) materials normalized to the value measured at 360 K.

Results

Resistivity Measurements. The macroscopic electrical properties of the iron-substituted materials were probed by variable-temperature resistivity measurements. Normalized resistance versus temperature curves for $x(Fe) = 0$–0.15 are shown in Figure 2. The absolute sample resistance determined at 350 K increases from 0.0039 to 0.096 Ω·cm as $x(Fe)$ increases from 0.01 to 0.15, respectively. These resistance versus temperature curves exhibit two distinct types of behavior depending on the concentration of iron. For $x(Fe) \leq 0.02$ a well-defined and abrupt change in the sample resistance is observed between 300 and 350 K (Figure 2A). This abrupt change in resistivity corresponds to the first-order incommensurate to nearly commensurate phase transition. The transition temperatures for these samples depend on the concentration of iron and are 355, 332, and 308 K for $x(Fe) = 0$, 0.01, and 0.02, respectively.[21] In contrast, for $x(Fe) \geq 0.04$ no abrupt (first-order) change in the sample resistance is observed between 350 and 100 K (Figure 1B). The absence of a resistance

(19) Wieder, H. H. *Laboratory Notes on Electrical and Galvanomagnetic Measurements*; Elsevier: New York, 1979.

(20) (a) Wu, X. L.; Lieber, C. M. *Proc. Natl. Acad. Sci. U.S.A.*, in press. (b) Thomson, R. E.; Walter, U.; Ganz, E.; Clarke, J.; Zettl, A.; Rauch, P.; DiSalvo, F. J. *Phys. Rev. B: Solid State* **1988**, *38*, 10734. (c) Drake, B.; Sonnenfeld, R.; Schneir, J.; Hansma, P. K.; Slough, G.; Coleman, R. V. *Rev. Sci. Instrum.* **1986**, *57*, 441.

(21) The transition temperature corresponds to the midpoint of the resistance anomaly associated with the incommensurate to nearly commensurate transition.

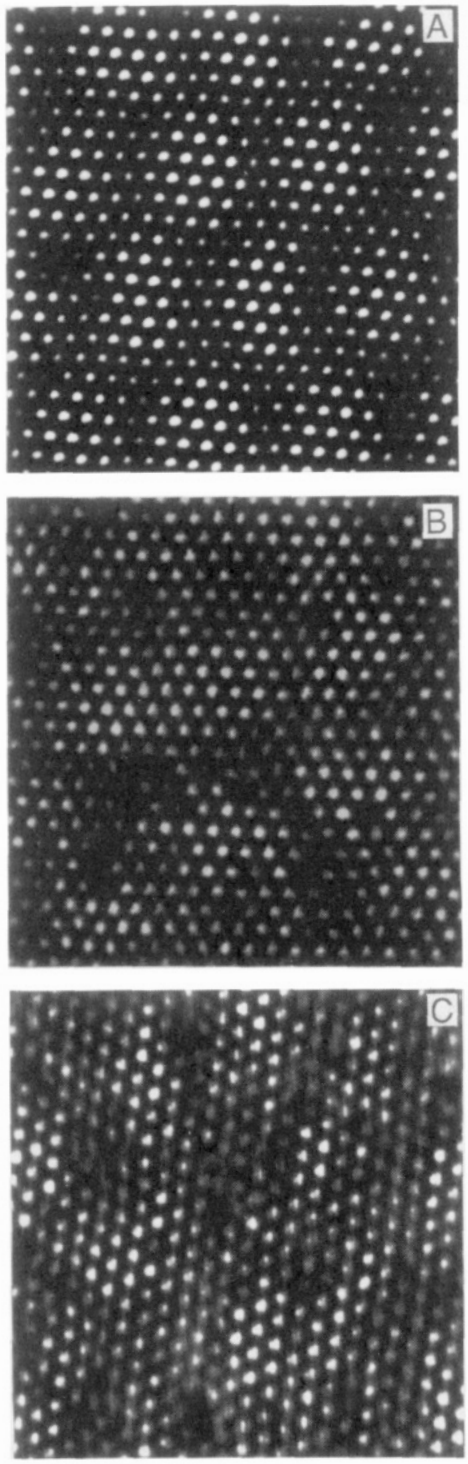

Figure 3. 240 × 240 Å^2 gray-scale images of (A) 1T-TaS_2, (B) $Fe_{0.01}Ta_{0.99}S_2$, and (C) $Fe_{0.02}Ta_{0.98}S_2$ recorded at room temperature with a 2-nA tunneling current and a 11-mV bias voltage.

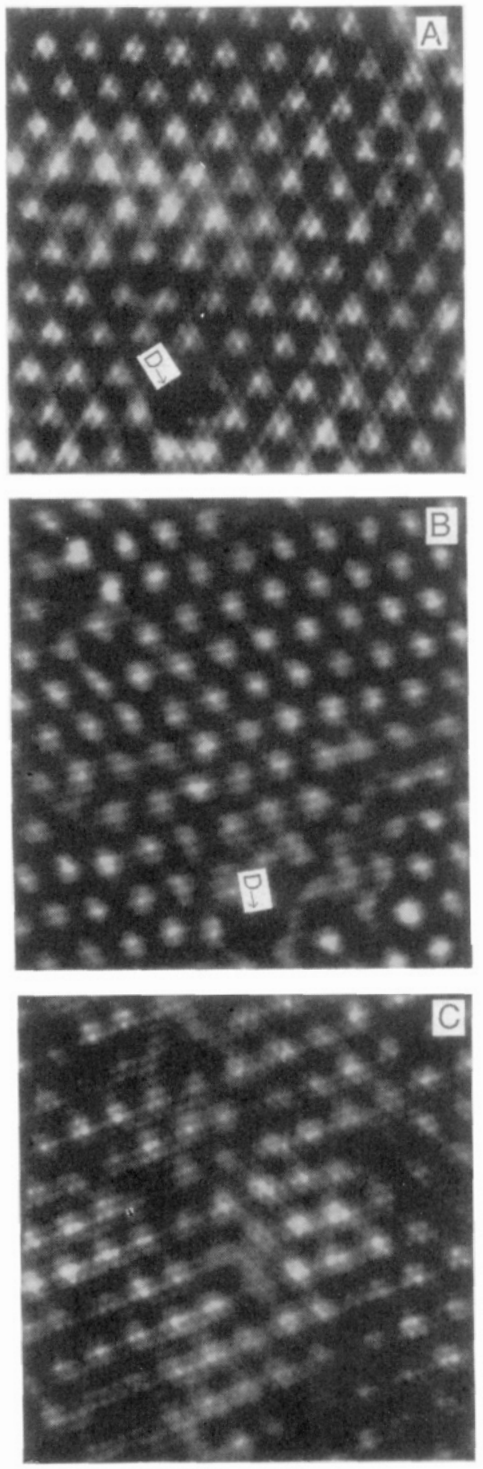

Figure 4. 120 × 120 Å^2 images of (A) 1T-TaS_2, (B) $Fe_{0.01}Ta_{0.99}S_2$, and (C) $Fe_{0.02}Ta_{0.98}S_2$ recorded with a 2-nA tunneling current and a 11-mV bias voltage at 359, 346, and 338 K, respectively. Several CDW defects are marked with "D" in (A) and (B).

anomaly in the $x(Fe) \geq 0.04$ crystals indicates that only the incommensurate CDW phase is stable in these materials. For the $x(Fe) \leq 0.02$ samples, however, either the incommensurate or the nearly commensurate phase may be stable, depending on the sample temperature. These results are similar to those reported previously by DiSalvo and co-workers.[17a]

Scanning Tunneling Microscopy. We have probed the origin of these macroscopic differences at the atomic scale with STM. Gray-scale images of 1T-TaS_2, $Fe_{0.01}Ta_{0.99}S_2$, and $Fe_{0.02}Ta_{0.98}S_2$ recorded at room temperature with a 2-nA tunneling current and a 11-mV bias voltage are shown in Figure 3. Tunneling images of 1T-TaS_2, $Fe_{0.01}Ta_{0.99}S_2$, and $Fe_{0.02}Ta_{0.98}S_2$ recorded at 359, 346, and 338 K, respectively, are shown in Figure 4. The white areas in these images represent surface protrusions and/or a high local density of states. Peaks corresponding to both the hexagonal CDW superlattice (period ≈12 Å) and the atomic lattice (period =3.35 Å) are resolved in these images. The resistance versus temperature curves (Figure 2A) indicate that the $x(Fe) = 0$, 0.01, and 0.02 materials are in the nearly commensurate state at room temperature and in the incommensurate state at 359, 346, and 338 K, respectively (i.e., the conditions used to record the images in Figure 4).

Both the CDW amplitude and the orientation of the CDW superlattice relative to the atomic lattice are different in images of the incommensurate versus the nearly commensurate phases (Figures 3 and 4). The CDW amplitude in the nearly commensurate phase exhibits a quasi-periodic modulation that defines

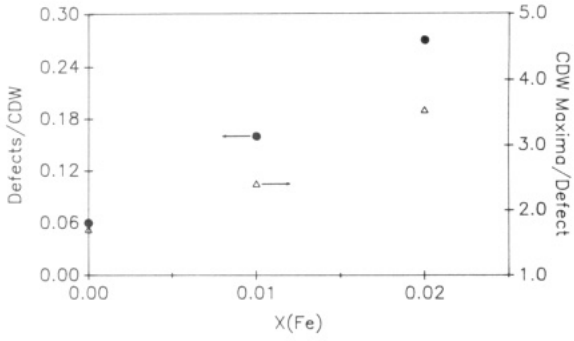

Figure 5. Plots of the frequency of CDW defects (●) and the size of these defects (△) versus the concentration of iron for samples in the incommensurate state.

approximately circular domains of high-amplitude CDW maxima separated by low-amplitude domain boundaries (Figure 3A).[16] This domain structure becomes increasingly disordered as x(Fe) increases from 0 to 0.02. In contrast, the amplitude of the CDW in the incommensurate state is more uniform (Figure 4A). The CDW superlattice also exhibits a different orientation relative to the lattice in the incommensurate versus the nearly commensurate phases. In the incommensurate phase the CDW superlattice and the atomic lattice vectors are coincident. Since the CDW wavelength is not an integral number of lattice periods, the CDW maxima are randomly oriented relative to the lattice sites in the incommensurate state (the CDW superlattice is itself ordered, however). In contrast, the CDW superlattice is rotated 12° on average relative to the atomic lattice in the nearly commensurate state.[22]

The images of the $Fe_xTa_{1-x}S_2$ ($x \leq 0.02$) materials also exhibit systematic changes in the CDW structure as x(Fe) increases from 0 to 0.02 in both the incommensurate and nearly commensurate phases. Further examination of the incommensurate phase images in Figure 4 shows that there are localized regions where the CDW amplitude is reduced relative to the rest of the image. These low-amplitude regions have been previously termed CDW defects.[18,23] Such defects could be due to the iron "impurity" sites in the lattice, surface contamination, or lattice vacancies. These latter two possibilities, however, are unlikely since the defect frequency is constant for a given value of x(Fe); the frequency and size of the defects increases with increasing x(Fe) (Figure 5), and the surface atomic lattice does not exhibit vacancies in the low-amplitude CDW regions. Hence, it is likely that the CDW defects are due to the iron centers that are substituted in the lattice. Similar defects are also apparent in images of the x(Fe) ≤ 0.02 materials recorded at room temperature. The frequency of these defects has not been characterized quantitatively, however, since CDW amplitude variations are intrinsic to the domainlike CDW phase in pure TaS_2 (see above).[16]

In addition to characterizing the size and frequency of the CDW defects in the incommensurate phase of the iron-substituted materials, atomic resolution images have been used to elucidate in detail the nature of these defects. A profile of the vertical corrugation across a typical defect for an x(Fe) = 0.01 sample is shown in Figure 6. For this defect the CDW corrugation is ≈0.8 Å lower than in the surrounding area. The 2-Å CDW corrugation and the 0.8-Å amplitude decrease at the defect site (Figure 6B) most likely correspond to variations in the charge density (density of states) and not to variations in the atomic positions.[9,11,14] Notably, the position of the CDW maxima in the defect region (Figure 6B) is shifted from that expected for an ideal sinusoidal CDW (Figure 6C); in other cases the CDW maxima may not shift from its ideal position. The phase of the CDW on either side of these defects, however, is the same regardless of the position in the defect region. These results indicate that a defect

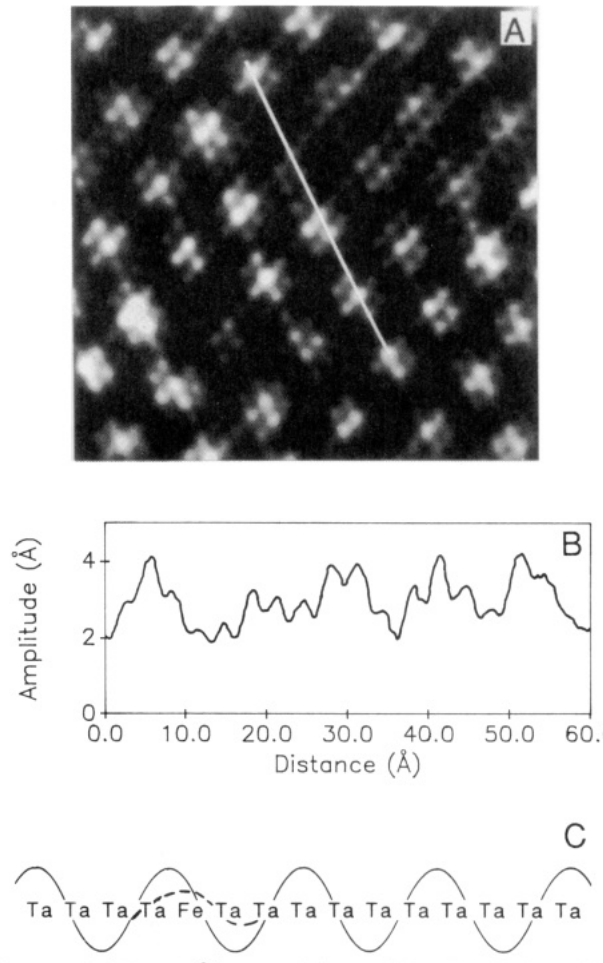

Figure 6. (A) 70 × 70 Å^2 gray-scale image of $Fe_{0.01}Ta_{0.99}S_2$ that exhibits several CDW defects. (B) Profile of the surface corrugation along the line marked in (A), crossing one defect. (C) Schematic view of the CDW defect that shows the location of an iron impurity in the lattice. A possible distortion of the ideal sinusoidal CDW (—) is indicated by the broken curve (- - -).

can be characterized as either an amplitude distortion or a coupled amplitude–position distortion that is spatially localized. Similar behavior is observed for the x(Fe) = 0.02 samples, although the typical defect size is larger than for the x(Fe) = 0.01 materials (Figure 5).

The substitution of iron at levels greater than 0.02 has also been investigated. Representative images of $Fe_{0.04}Ta_{0.96}S_2$, $Fe_{0.08}Ta_{0.92}S_2$, $Fe_{0.15}Ta_{0.85}S_2$, and $Fe_{0.2}Ta_{0.8}S_2$ are shown in Figure 7. Since the incommensurate to nearly commensurate phase transition was not observed in the resistivity measurements made on these samples (Figure 2B), it is expected that the CDW phase is incommensurate. We find that as x(Fe) increases from 0.04, the CDW superlattice becomes increasingly irregular (nonhexagonal) until at x(Fe) = 0.20 the CDW modulation is no longer detected by STM (Figure 6D).[24] Previously, the CDW phase was not clearly detected for x(Fe) > 0.1 in electron diffraction experiments.[17a,b] The CDW structure for the $0.04 \leq x(\text{Fe}) \leq 0.15$ materials determined from the STM images consists of small clusters of high-amplitude CDW maxima and areas where the CDW amplitude is lower and the maxima are not well-defined. The variation in the CDW amplitude between these two regions is approximately 1 Å. The high-amplitude clusters are irregular in size and shape, although in general their size decreases as x(Fe) increases from 0.04 to 0.15. Notably, the CDW-atomic lattice orientation angle in these high-amplitude regions is often greater than the 0° orientation angle expected for an incommensurate phase.

(22) For a complete discussion of the structure of the nearly commensurate phase see ref 16.

(23) Giambattista, B.; Johnson, A.; Coleman, R. V.; Drake, B.; Hansma, P. K. *Phys. Rev. B: Solid State* **1988**, *37*, 2741.

(24) The $Fe_{0.2}Ta_{0.8}S_2$ samples were generously donated by J. V. Waszczak, AT&T Bell Laboratories.

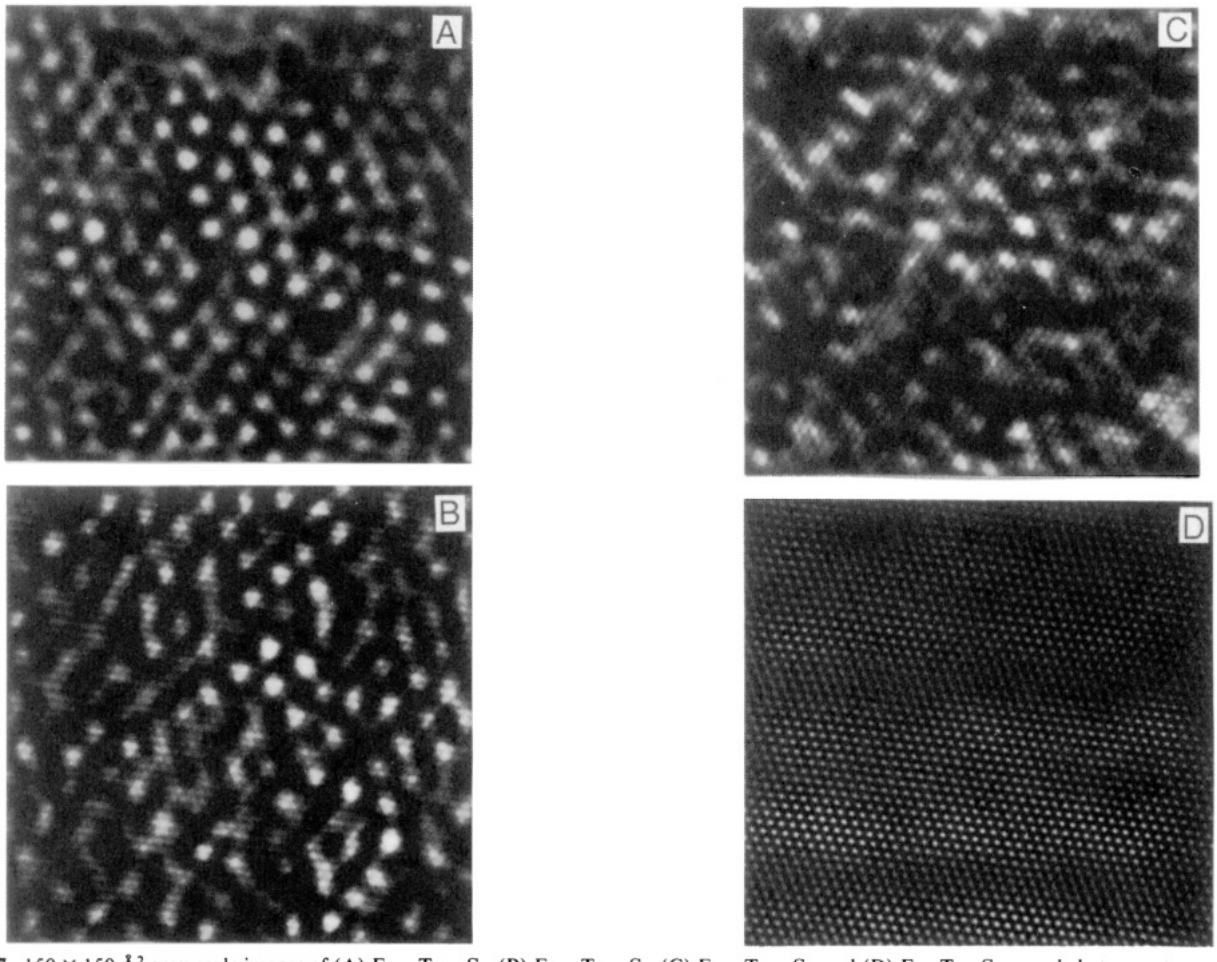

Figure 7. 150 × 150 Å^2 gray-scale images of (A) $Fe_{0.04}Ta_{0.96}S_2$, (B) $Fe_{0.08}Ta_{0.92}S_2$, (C) $Fe_{0.15}Ta_{0.85}S_2$, and (D) $Fe_{0.2}Ta_{0.8}S_2$ recorded at room temperature with a 2-nA tunneling current and a 11-mV bias voltage.

In addition, real-space wavelength measurements and the two-dimensional Fourier transform (2DFT) power spectrum of the image data have been used to analyze the disorder in the superlattice of the x(Fe) = 0.04–0.15 images. The average CDW wavelength determined from images of the $Fe_xTa_{1-x}S_2$ materials is plotted as a function of x(Fe) in Figure 8A. The wavelength measurements were averaged from at least six incommensurate phase images for each iron concentration and are found to increase 2.1 Å as x(Fe) increases from 0 to 0.15.[25] The standard deviation (σ) in these average wavelength measurements provides an estimate of the magnitude of the distortion in the CDW superlattice.[11b] The value of σ determined from the wavelength measurements is plotted as a function of x(Fe) in Figure 8B. This figure demonstrates that there is a significant increase in the CDW wavelength distortions for x(Fe) > 0.02.

The 2DFT power spectra of images of the x(Fe) = 0, 0.04, 0.15, and 0.20 samples are shown in Figure 9. The power spectrum for the pure material (Figure 9A) exhibits two sets of peaks that correspond to the first-order CDW (C) and lattice (L) peaks. The six CDW and six lattice peaks reflect the hexagonal symmetry of the superlattice and the atomic lattice. In the iron-substituted materials the six lattice peaks remain well-defined; however, a diffuse ring of intensity is observed at the CDW positions as x(Fe) increases to 0.15. The diffuse ring is consistent with a distorted CDW superlattice (see below). In contrast, only the six atomic lattice peaks are observed in a 2DFT power spectrum for the x(Fe) = 0.2 material (Figure 9D).

Discussion

Random substitution of the tantalum sites with other metal centers produces disorder in the lattice potential.[7] Previous results

(25) The origin of the increase in the average wavelength determined from our data will be discussed elsewhere: Chen, H.; Lieber, C. M., In preparation.

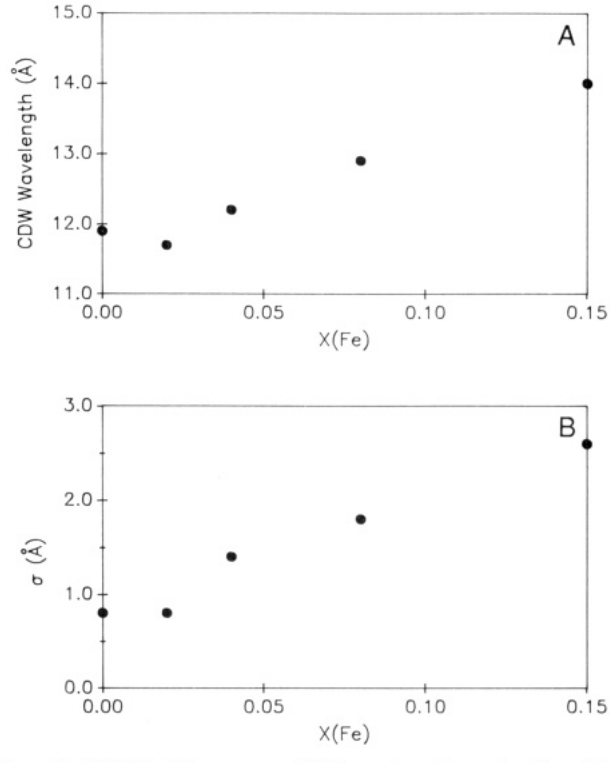

Figure 8. (A) Plot of the average CDW wavelength as a function of the concentration of iron. (B) Plot of the standard deviation (σ) for the average wavelength measurements as a function of x(Fe). The σ determined for the x(Fe) = 0 material represents the uncertainty intrinsic to these measurements.

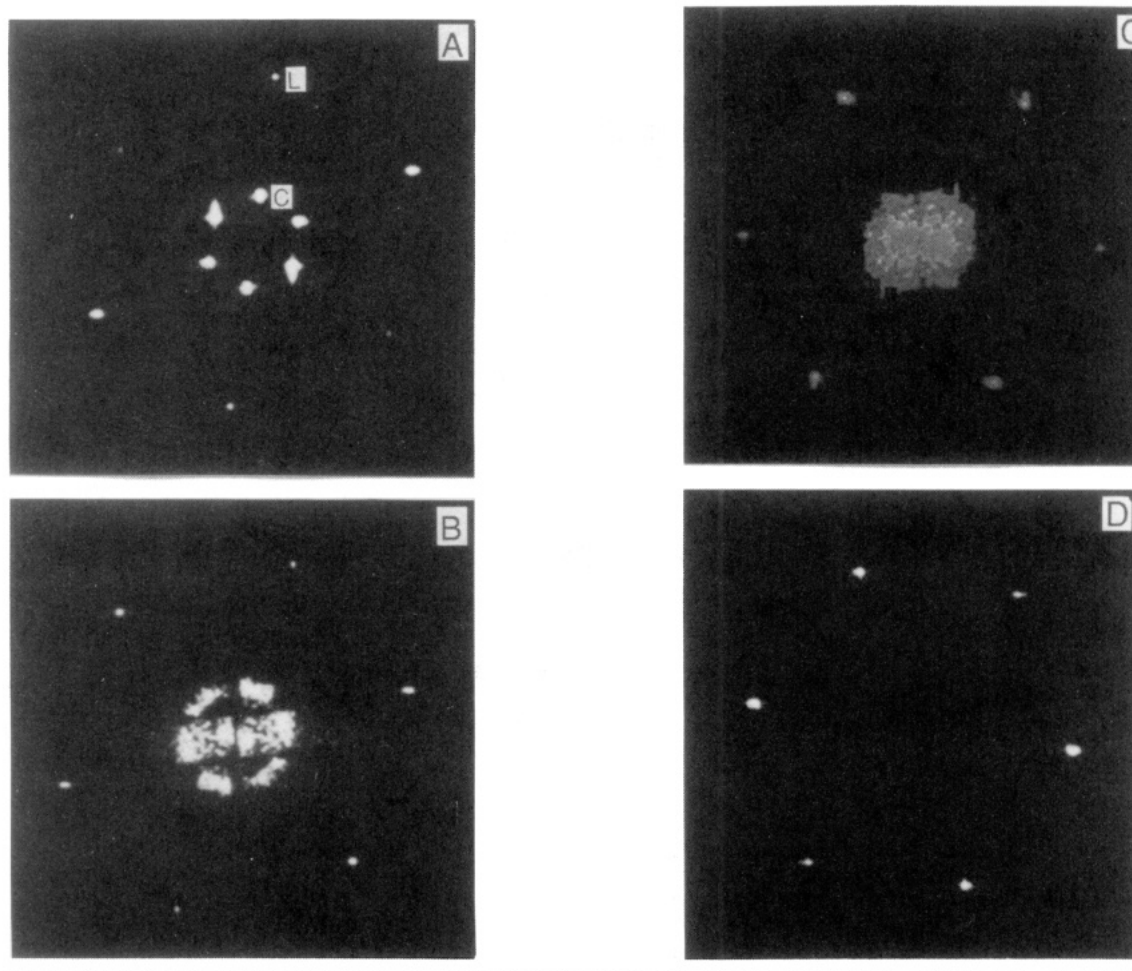

Figure 9. Typical two-dimensional Fourier transform power spectra of images recorded for the (A) 1T-TaS_2, (B) $Fe_{0.04}Ta_{0.96}S_2$, (C) $Fe_{0.15}Ta_{0.85}S_2$, and (D) $Fe_{0.2}Ta_{0.8}S_2$ materials. CDW and atomic lattice peaks are marked in (A) with a "C" and "L", respectively.

from transport and diffraction studies indicate that in general metal substitution will drive the CDW to the incommensurate state.[7,14] This study and our other recent investigations of titanium- and niobium-substituted TaS_2[11,12] suggest that on the atomic level the response of the CDW phase to the metal impurities is more complicated.

The images of the iron-substituted materials show that the incommensurate phase has distinct characteristics for $x(Fe) \leq 0.02$ versus $x(Fe) > 0.02$. The incommensurate CDW phase exhibits a regular hexagonal structure similar to that indicated by previous diffraction experiments for $x(Fe) \leq 0.02$.[14,17] We have also shown, however, that there are well-defined defects in the incommensurate CDW superlattice (Figure 4). Since the frequency and size of these defects depend directly on the iron concentration (Figure 5), it is reasonable to attribute them to localized distortions of the CDW in response to the Fe sites as shown schematically in Figure 6C.[7,11] These spatially localized defects, which involve either a CDW amplitude distortion or a coupled amplitude–position distortion, will relax the CDW around the impurity sites and lower the energy of the system.[18,26] Notably, our results represent the first direct characterization of the amplitude and phase of defects in an incommensurate CDW phase; such data have been heretofore unavailable from previous studies (e.g., diffraction). To locate directly the positions of the iron sites in the lattice, however, will require additional experiments.[27]

For $x(Fe) \geq 0.04$ the microscopic CDW structure differs from the regular hexagonal incommensurate phase suggested on the basis of diffraction and transport experiments.[14,17] Our real-space STM images show that the intralayer CDW structure exhibits irregular distortions in the amplitude and wavelength (Figures 7 and 8). The 2DFT power spectra for the $x(Fe) \geq 0.04$ materials exhibit diffuse intensity around the CDW positions. Previously, diffuse scattering observed in diffraction studies has been attributed to the hexagonal incommensurate phase.[7,14,17] Our real-space images indicate, however, that this diffuse scattering should be attributed to variations in the CDW amplitude and wavelength. In addition, analysis of the STM images has shown that the variations in the CDW wavelength are significantly larger for the $x(Fe) \geq 0.04$ materials than the $x(Fe) \leq 0.02$ materials (Figure 8). These results suggest that for an iron concentration exceeding $x = 0.02$ the CDW–iron interaction energy is greater than the energy required to distort the CDW superlattice.[26]

It is also important to consider why both the macroscopic electrical properties (Figure 2) and microscopic CDW structure (Figures 4 and 7) differ significantly when $x(Fe) \leq 0.02$ versus $x(Fe) \geq 0.04$. For $x(Fe) \leq 0.02$ there are 0.26 iron impurity centers/CDW maxima since 13 metal sites can be associated with each CDW maxima in tantalum disulfide.[9b,14] Magnetic susceptibility and Mössbauer studies[17b] show, however, that iron substitutes as low-spin Fe(II) in TaS_2. Hence, two d^1-Ta(IV) centers must be oxidized to d^0-Ta(V) to maintain charge neutrality. This indicates that each iron center effectively creates a total of three impurities, so that for $x(Fe) = 0.02$ there is close to one impurity/CDW maxima. We suggest that this impurity level represents a critical concentration for TaS_2 that is independent of the chemical identity of the impurity. In support of our proposal, we note that substitution of Ti(IV) and Nb(IV) in TaS_2 at a level of $x(M) \approx 0.08$ leads to a significant change in the characteristics of the macroscopic electrical properties[7,14] and microscopic CDW structure.[11,12] At this level of substitution there is one Nb or Ti impurity/CDW maxima, since substitution of Ta(IV) sites with M(IV) species corresponds to one impurity/metal center.

(26) McMillan, W. L. *Phys. Rev. B: Condens. Matter* **1975**, *12*, 1187.
(27) Chen, H.; Lieber, C. M. Work in progresss.

Conclusions

In summary, the microscopic structural and electronic properties of the CDW phases in a series of iron-substituted tantalum disulfide materials, $Fe_xTa_{1-x}S_2$, have been characterized with STM. For $x(Fe) \leq 0.02$ the incommensurate CDW phase exhibits a regular hexagonal superlattice similar to that suggested on the basis of diffraction experiments. At the atomic level, however, these real-space STM studies show that there are also well-defined defects in this CDW structure. These defects, which are due to the iron centers in the lattice, involve a spatially localized amplitude distortion or coupled amplitude–phase distortion of the CDW. For $0.04 \leq x(Fe) \leq 0.15$ the CDW superlattice exhibits large variations in the wavelength and amplitude in contrast to the hexagonal incommensurate phase suggested from diffraction studies. The origin of these differences between the STM and diffraction results has been resolved from the analysis of 2DFT power spectra of our images and real-space wavelength measurements. In addition, we have shown that these results and our previous studies of metal substitution suggest that there is a critical impurity level corresponding to one impurity/CDW maxima for substitution in the tantalum disulfide system.

Acknowledgment. We thank Jin-Lin Huang for helpful discussions. C.M.L. acknowledges support of this work by The David and Lucile Packard Foundation, the Air Force Office of Scientific Research (Grant AFOSR-90-0029), the National Science Foundation (Grant CHE-8857194), and Rohm and Haas Co.

Reactions of Boron Atoms and Clusters with Methane, Methyl Bromide, and Water under Matrix Isolation Conditions

G. H. Jeong,[1] R. Boucher, and K. J. Klabunde*

Contribution from the Department of Chemistry, Kansas State University, Manhattan, Kansas 66506. *Received February 13, 1989. Revised Manuscript Received November 30, 1989*

Abstract: Boron was evaporated with a pulsed XeCl excimer laser, and the vapor cocondensed on a cold window (near 10 K) with argon mixtures of CH_4, CH_3Br, and H_2O, and ^{13}C and ^2H labeled analogues. Consumption of B and B_2 was monitored by UV–vis spectroscopy, and reaction products were monitored with FT-IR. Atom insertion products H_3CBH, H_3CBBr, and HOBH were detected. Evidence was found for B_2 reactions with CH_4 and CH_3Br, suggesting the formation of dinuclear bridged hydrogen species. Larger boron clusters were detected by FT-IR, which were unreactive with CH_4 and, in one case, with water.

Boron atom chemistry has interested scientists for many years. Progress has been slow, however, due to the difficulty in producing atoms from the solid. Timms,[2] employing electron beam evaporation of boron, studied boron atom interactions with hydrogen halides and found HBX_2 (X = Cl, Br) as products, which were probably formed through a series of free radical reactions. McGlinchey, Brent, and Skell[3] reported oxidative addition reactions of boron atoms, for example with bromobenzene, C_6H_5-BBr_2 was formed. Also, water reacted to eventually yield $B(OH)_3$ under the conditions of the experiment (codeposition at 77 K followed by warming). More recent gas-phase studies of B atom/H_2O interactions by Gole and Pace[4] indicated the formation of BO*. Sakai and Jordan,[5] using theoretical approaches, predict that the HOBH molecule should be bound by at least 90 kcal/mol with respect to B and H_2O. Further work by Sakai and Jordan[6] suggests that B–H_2O reactions should proceed with a small E_a for the insertion reaction

$$B + H_2O \rightarrow B{\cdot}OH_2 \xrightarrow{E_a = 12\ \text{kcal}} HOBH \rightarrow BO^* + H_2$$

thus, HOBH should be experimentally detectable, although in the gas phase excited HOBH decomposes to BO and H_2.

Other gas-phase studies of B atoms with oxygen compounds have appeared.[7-9] Oxygen abstraction is the main reaction channel yielding excited-state BO. No direct evidence for insertion products ROBH, HOBH, or similar species has been obtained, except from our earlier study of the matrix B–CH_4 reaction, which indicated the matrix isolation of H_3CBH.[10] This work followed earlier work with Al and other metal atoms with CH_4 and CH_3Br.[11,12] The earlier work[11] attracted the attention of Lebrilla and Maier,[13] who carried out theoretical calculations on the reactions of B^+, B, B^-, C, and Al with CH_4, which predicted that very low activation energies should be encountered for the reactions of B atoms, B^-, C atoms, and Al atoms with C–H bonds. Their conclusion was that C–H activation should be a facile process if the attacking reagent has an electronic structure similar to that of a carbene: one empty orbital and one filled or partially filled orbital each of p-type symmetry.

With this background we began a more in depth study of the low-temperature reactions of B atoms/clusters with CH_4, CH_3Br, and H_2O. In our study we employed a pulsed XeCl excimer laser to evaporate boron. Since we were most interested in ground-state reactions of B atoms, we took precautions to ensure that electronically excited boron species would not live long enough to reach the reaction zone. Thus, we fashioned an apparatus where a 5-cm distance separated the boron rod and the trapping window.[10]

(1) Present address: Busan National University, Department of Chemistry, Busan, 609-735 Korea.
(2) Timms, P. L. *Chem. Commun.* **1968**, 258–259.
(3) McGlinchey, M.; Skell, P. S. In *Cryochemistry*; Moskovits, M., Ozin, G., Eds.; Wiley-Interscience: New York; pp 153–155. Brent, W. N. Ph.D. Thesis, Pennsylvania State University, 1974.
(4) Gole, J. L.; Pace, S. A. *J. Phys. Chem.* **1981**, *85*, 2651–2655.
(5) Sakai, S.; Jordan, K. D. *Chem. Phys. Lett.* **1986**, *130*, 103–110.
(6) Sakai, S.; Jordan, K. D. *J. Phys. Chem.* **1983**, *87*, 2293–2295.
(7) Tobacco, M. B.; Stanton, C. T.; Davidovits, P. *J. Phys. Chem.* **1986**, *90*, 2765–2768.
(8) DiGluseppi, T. G.; Estes, R.; Davidovits, P. *J. Phys. Chem.* **1982**, *86*, 260–262.
(9) DeHaven, J.; O'Connor, M. T.; Davidovits, P. *J. Phys. Chem.* **1981**, *75*, 1746–1751.
(10) Klabunde, K. J.; Jeong, G. H. *J. Am. Chem. Soc.* **1986**, *108*, 7103–7104.
(11) Klabunde, K. J.; Tanaka, Y. *J. Am. Chem. Soc.* **1983**, *105*, 3544–3546.
(12) Parnis, J. M.; Ozin, G. A. *J. Am. Chem. Soc.* **1986**, *108*, 1699–1700.
(13) Lebrilla, C. B.; Maier, W. F. *Chem. Phys. Lett.* **1984**, *105*, 183–188.

0002-7863/90/1512-3332$02.50/0